AMERICAN SOCIETY FOR MICROBIOLOGY | Antimicrobial Agents and Chemotherapy®

EXPERIMENTAL THERAPEUTICS

Whole-Cell Phenotypic Screening of Medicines for Malaria Venture Pathogen Box Identifies Specific Inhibitors of *Plasmodium falciparum* Late-Stage Development and Egress

Alok Tanala Patra,[a] Tejashri Hingamire,[b,c] Meenakshi A. Belekar,[b,c] Aoli Xiong,[d] Gowtham Subramanian,[a] Zbynek Bozdech,[e] Peter Preiser,[e] Dhanasekaran Shanmugam,[b,c] Rajesh Chandramohanadas[a]

[a]Pillar of Engineering Product Development (EPD), Singapore University of Technology and Design (SUTD), Singapore
[b]Biochemical Sciences Division, CSIR National Chemical Laboratory, Pune, India
[c]Academy of Scientific and Innovative Research, Ghaziabad, India
[d]BioSystems and Micromechanics (BioSyM)—IRG, Singapore MIT Alliance for Research & Technology Centre, Singapore
[e]School of the Biological Sciences, Nanyang Technological University, Singapore

ABSTRACT We report a systematic, cellular phenotype-based antimalarial screening of the Medicines for Malaria Venture Pathogen Box collection, which facilitated the identification of specific blockers of late-stage intraerythrocytic development of *Plasmodium falciparum*. First, from standard growth inhibition assays, we identified 173 molecules with antimalarial activity (50% effective concentration [EC_{50}] $\leq$ 10 μM), which included 62 additional molecules over previously known antimalarial candidates from the Pathogen Box. We identified 90 molecules with EC_{50} of $\leq$1 μM, which had significant effect on the ring-trophozoite transition, while 9 molecules inhibited the trophozoite-schizont transition and 21 molecules inhibited the schizont-ring transition (with $\geq$50% parasites failing to proceed to the next stage) at 1 μM. We therefore rescreened all 173 molecules and validated hits in microscopy to prioritize 12 hits as selective blockers of the schizont-ring transition. Seven of these molecules inhibited the calcium ionophore-induced egress of *Toxoplasma gondii*, a related apicomplexan parasite, suggesting that the inhibitors may be acting via a conserved mechanism which could be further exploited for target identification studies. We demonstrate that two molecules, MMV020670 and MMV026356, identified as schizont inhibitors in our screens, induce the fragmentation of DNA in merozoites, thereby impairing their ability to egress and invade. Further mechanistic studies would facilitate the therapeutic exploitation of these molecules as broadly active inhibitors targeting late-stage development and egress of apicomplexan parasites relevant to human health.

KEYWORDS phenotypic screening, *Plasmodium falciparum*, Medicines for Malaria Venture, Pathogen Box, stage-specific inhibition, egress, DNA fragmentation, MMV, schizonts

Despite technological advancements and improved knowledge of disease manifestation and pathogen biology, progress in the development of novel therapeutics has been slower than expected for malaria. In this context, repurposing of old drugs with established mechanisms is becoming a viable alternative with the potential for shortening the time window from efficacy testing to pharmacophore optimization (1–3) and eventual application. In an effort to speed up the process of drug development against malaria and other pathogenic organisms, a collaborative model of public-private partnerships (PPPs) facilitated through the Medicines for Malaria Venture (MMV; mmv.org) was formed. As an outcome of this program, well-characterized small-

Citation Patra AT, Hingamire T, Belekar MA, Xiong A, Subramanian G, Bozdech Z, Preiser P, Shanmugam D, Chandramohanadas R. 2020. Whole-cell phenotypic screening of Medicines for Malaria Venture Pathogen Box identifies specific inhibitors of *Plasmodium falciparum* late-stage development and egress. Antimicrob Agents Chemother 64:e01802-19. https://doi.org/10.1128/AAC.01802-19.

Address correspondence to Dhanasekaran Shanmugam, d.shanmugam@ncl.res.in, or Rajesh Chandramohanadas, rajesh@sutd.edu.sg.

Received 3 September 2019
Returned for modification 6 October 2019
Accepted 10 February 2020
Accepted manuscript posted online 18 February 2020
Published 21 April 2020

molecule libraries were made accessible to academics worldwide for the purpose of identifying novel bioactivities and pursuing mechanistic and efficacy studies. In 2015, the consortium launched the open access Pathogen Box, consisting of 400 drug-like small molecules (including 26 reference compounds) with confirmed bioactivity against at least one of several neglected disease pathogens (4).

Open access to the Pathogen Box resulted in the assignment of new activities for the inhibitors in this chemical library. For example, MMV688934 (tolfenpyrad) was recently shown to be active against the helminth parasite and barber's pole worm (5), while MMV688768 was found to inhibit biofilm formation by *Candida albicans* (6). These two molecules were previously established as inhibitors of kinetoplastid and schistosome parasites (5, 6), respectively. However, the latter molecule has recently been documented to have no activity against *Schistosoma mansoni* (7). Dual activity against *Giardia* and *Cryptosporidium* was reported for MMV010576, MMV028694, and MMV676501, which showed ≥75% inhibitory efficacy (8). Several such studies have accelerated the identification of potent molecules that have now been reprofiled, repurposed, and reclassified to show broader inhibitory activities against more than one pathogenic agent (9–12).

Among the plasmodia causing malaria in humans, *Plasmodium falciparum* is the most widespread and virulent form, accounting for 99.7% of estimated malaria cases in the African region, 62.8% in Southeast Asia, 69% in the Eastern Mediterranean region, and 71.9% in the Western Pacific region (13–15). Within the human host, *Plasmodium* undergoes vastly different developmental processes in liver cells and red blood cells (RBCs). However, intraerythrocytic (blood-stage) development is responsible for transmission, parasite density, and, therefore, malaria-associated pathological outcomes. Over the past several decades, attempts to eradicate malaria have had some success, but challenges remain, especially in the form of drug resistance, multispecies infections, and changes in vector distribution and density. Regions where malaria is endemic are rapidly losing affordable and effective therapeutic options, making it necessary to develop new drugs with novel modes of action.

In this work, we determined the stage-specific inhibitory activity of Pathogen Box molecules against *P. falciparum* asexual development through a phenotype-based screening approach. First, growth inhibition assays were carried out to assess the antimalarial potential of all 400 molecules. In addition to confirming the activity of the antimalarial molecules that were originally listed by MMV, 62 additional molecules were identified for antimalarial activity, of which 38 overlapped with a recent study (10). Inhibitors exhibiting a 50% effective concentration (EC_{50}) of ≤1 μM (90 molecules) were selected for further evaluation of their stage-specific inhibition across blood-stage *P. falciparum* development. This evaluation identified 9 molecules that inhibited trophozoite development and 21 molecules that inhibited schizont-ring ([S→R]) transition. Upon rescreening of the 173 active molecules (identified in this study) for their activities against schizonts, 12 molecules that selectively impaired the schizont-ring transition and egress of merozoites from infected RBCs were prioritized. Interestingly, 7 of these molecules were also inhibitory to calcium ionophore-induced egress of tachyzoite-stage *Toxoplasma gondii*, suggesting a likely conserved mechanism of action affecting parasite egress from host cells. We demonstrate that two of these molecules affect the integrity of merozoite DNA, while others appear to interfere directly with the egress process. These findings provide new starting points for mechanistic studies toward the development of new therapies to treat malaria and toxoplasmosis.

RESULTS AND DISCUSSION

Antimalarial activity profiling of MMV Pathogen Box molecules. Among the 400 antiparasitic molecules in the MMV Pathogen Box, 123 were originally reported to be active against blood-stage malaria parasites (3D7 strain), and of these, 72 molecules exhibited potency at nanomolar concentrations ($EC_{50} < 1$ μM; source, mmv.org/mmv-open/pathogen-box). However, additional molecules with potent antimalarial activity are likely to be present in the Pathogen Box collection, as reported in recent studies

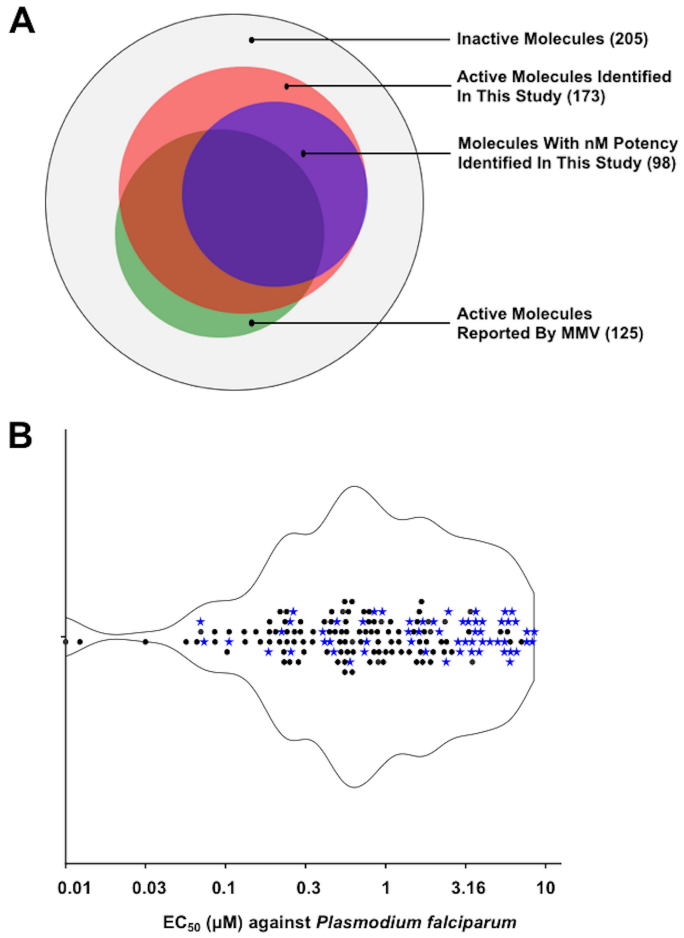

FIG 1 Identifying Pathogen Box molecules inhibiting the growth of blood-stage *P. falciparum* parasites. (A) Segregation of molecules based on their antimalarial activity. From the Pathogen box library, we identified 173 molecules that inhibited parasite growth by ≥80% at a 10 μM concentration (shown in red). Out of these, 98 molecules showed potency against blood-stage *P. falciparum* parasites at nanomolar concentrations (indicated in blue). Although 125 molecules (including the reference compounds) are expected to possess antimalarial activity based on MMV data (indicated in green), 24 molecules showed only moderate potency (≥50%) at 10 μM in our screens. (B) EC_{50} values for the 173 molecules with antimalarial activity are presented to show their potency distribution. Newly identified molecules with antimalarial activity (from this study) are indicated in blue.

(10, 12, 16, 17). It is apparent from these studies that the inhibitors can have shared or distinct phenotypic effects on different life cycle stages of *Plasmodium* spp., which formed the motivation for this study.

To discover novel antimalarials from the collection and to validate the reported activities, we employed a systematic screening approach. First, using a standard endpoint growth inhibition assay, all molecules from the Pathogen Box were tested at a 10 μM concentration for their activity against blood-stage *P. falciparum* (3D7 strain), and those affecting parasite growth inhibition by ≥80% were selected for EC_{50} determination. A total of 173 molecules (~43% hit rate) were found to inhibit the growth of *P. falciparum* parasites by ≥80%. Of the 125 molecules originally included as antimalarials by MMV, only 101 showed ≥80% inhibition of parasite growth (Fig. 1A), and the remaining 24 had lower levels of inhibitory activity, presumably due to differences in the assay conditions (10). A compilation of the antimalarial screening data for all Pathogen Box molecules is provided in Data Set S1 in the supplemental material.

Interestingly, 72 molecules previously shown to be active against other pathogens were found to possess antimalarial activity, with several of them showing potency at nanomolar concentrations (Fig. 1B). For instance, antikinetoplastid molecules like

MMV688362 and MMV688271 inhibited *P. falciparum* growth with potency at nanomolar concentrations ($EC_{50} \leq 0.4\ \mu M$). These molecules are predicted to bind to the minor groove at AT-rich regions of DNA in other organisms (18, 19), which may render them with inhibitory potential against multiple pathogens. Furthermore, MMV652003 and MMV688283, which are members of the benzamide 4-quinolinamine class of compounds and which are predicted to target leucyl-tRNA synthetase and β-hematin formation, respectively (20, 21), were positively identified to be antimalarial hits. Another compound, MMV675968, which has chemical features similar to those of inhibitors of dihydrofolate reductase (DHFR) in *Cryptosporidium* and *Toxoplasma* (8, 11), displayed potent antimalarial activity with an estimated EC_{50} of 0.07 μM. Therefore, it is likely that this molecule may target the DHFR enzyme in *P. falciparum* (22). MMV671636, a quinolinone-class molecule with antifilarial activity, showed very potent antimalarial activity with an estimated EC_{50} of 0.01 μM. This compound is predicted to target the mitochondrial cytochrome bc_1 complex, making it a promising candidate for chemoprophylaxis treatment of malaria (23, 24). Molecules previously shown to be active against *Mycobacterium tuberculosis*, such as MMV021660 (guanidine) and MMV687765 (pyrimidine), with EC_{50} values of 0.07 and 0.47 μM, respectively, also inhibited *P. falciparum* in our screens. Although their mechanism of action against *P. falciparum* remains unknown, these molecules are known to disrupt the folate pathway and tyrosine kinase activities in *M. tuberculosis* (25, 26). Several other compounds, such as MMV688943, MMV688371, MMV688274, MMV688754, MMV688273, MMV688550, MMV023969, MMV495543, MMV637229, MMV668727, MMV676063, MMV688761, MMV688763, MMV688552, and MMV688509, belonging to the sets of agents in Pathogen Box with activity against kinetoplastids, tuberculosis, hookworm infections, filariasis, schistosomiasis, and toxoplasmosis disease, showed efficacy against *P. falciparum* at submicromolar to micromolar concentrations and warrant further consideration.

Segregation of Pathogen Box molecules by stage-specific inhibition of *P. falciparum*. Conventional growth inhibition assays with *P. falciparum* do not capture the parasite stage-specific effects of inhibitory molecules. This remains a challenge, since drug sensitivity can vary substantially during the 48-h blood-stage developmental cycle and can be influenced by the metabolic fate of the drugs under prolonged *in vitro* conditions, leading to alterations to the pharmacodynamic properties (27, 28). Therefore, to further categorize the Pathogen Box molecules by stage-specific inhibitory potential, the 90 most potent molecules ($EC_{50} \leq 1\ \mu M$; Fig. 1B) were examined through phenotype screening (Fig. S2). Progressive developmental stages of parasites—rings (6 to 10 h postinfection [hpi]), trophozoites (20 to 22 hpi), and schizonts (40 to 42 hpi)—were treated with 1 μM inhibitor and assessed by flow cytometry after ~12 h for their ability to block stage transition (Fig. 2A). None of the molecules showed significant inhibition of the ring-trophozoite ([R→T]) transition, which is in line with previous reports suggesting that ring-stage parasites are rather resilient to antimalarial compounds (29, 30). Twenty newly identified molecules with EC_{50} values of $\leq 1\ \mu M$ (Fig. 2A, highlighted in blue) were part of the stage transition inhibition assay which showed various degrees of inhibition for trophozoite-schizont ([T→S]) and schizont-ring ([S→R]) transitions. For instance, we observed that MMV688271 (guanidine) had no effect on the [T→S] transition, although it is known to target the mitochondrial cytochrome *bc*1 complex. Two other molecules, MMV688754 and MMV675968, for which mechanistic insights are limited, were found to block the [T→S] and [S→R] transitions. Since trophozoites are engaged in a variety of metabolic activities essential for parasite survival and proliferation, they may offer more target options than the more quiescent ring-stage parasites. Furthermore, trophozoites are also transcriptionally more active and are engaged in the preparation of daughter cell formation and cell division, which make them target rich for small-molecule inhibitors (31, 32). Interestingly, we identified 20 molecules which had a significant effect on the [S→R] transition. Among them, MMV021660 is known to inhibit the folate pathway in *Mycobacterium* (33, 34). It is noteworthy that although the EC_{50} values for some of the newly identified antiplasmodial molecules (MMV637229, MMV024311, MMV687812, MMV687765, MMV652003,

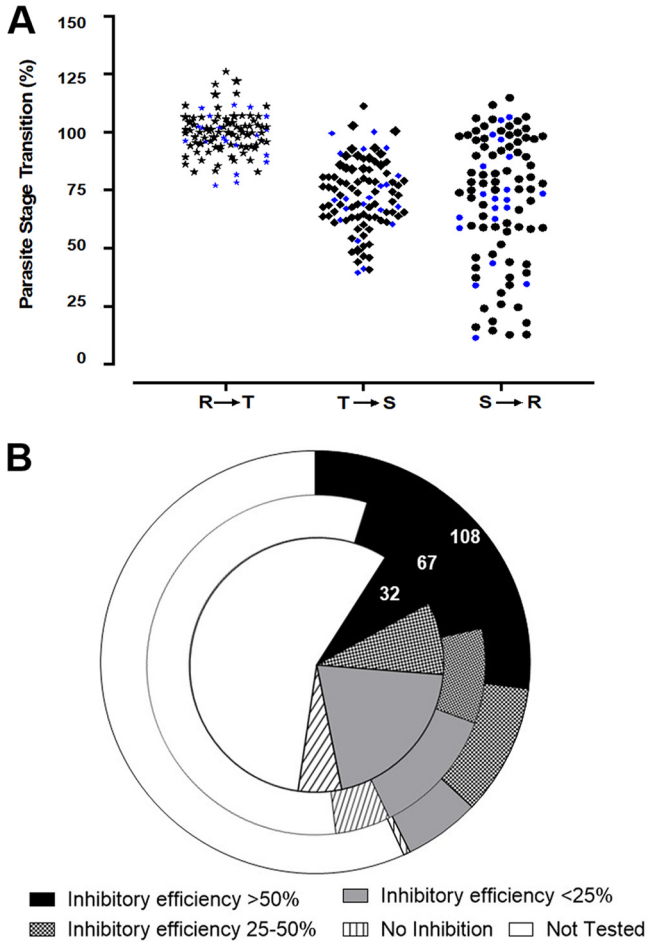

FIG 2 Stage-specific segregation of antimalarial activity for selected Pathogen Box molecules. (A) Flow cytometry data showing the percentage of parasites which successfully transitioned from ring to trophozoite [R→T], trophozoite to schizont [T→S], and schizont to ring [S→R]. Highlighted in blue are the molecules with antimalarial activity newly identified in this study. (B) Pie chart showing the inhibition of *P. falciparum* schizont-to-ring transition upon treatment with 10 μM (outer ring), 3 μM (middle ring), and 1 μM (inner ring) drug concentrations (showing an inhibitory efficiency of <25%, 25% to 50%, >50%, and no inhibition). At 10 μM, nearly 30% of the molecules affected the [S→R] transition, which was reduced to 15% and 8% at 3 and 1 μM, respectively, indicating an increase in the selectivity of the hits.

MMV676600, MMV688271, MMV688279, MMV688362) were in the nanomolar range, their stage-specific inhibitory efficiencies were quite varied and distinct. Our observations highlight that for most inhibitors, the overall potency of the inhibitor (expressed as the EC_{50}), as determined from 60-h growth inhibition assays, does not correlate with its stage-specific effect. The ability of ring-stage parasites to tolerate drug exposure and facilitate the emergence of drug resistance is documented (31). Thus, it is necessary to carefully study the progressive developmental response following inhibitor treatment.

Validation of molecules affecting the schizont-to-ring transition. Based on the results from the stage transition assays, we identified 20 molecules which showed inhibition of the [S→R] transition. In order to avoid missing out on other potential [S→R] inhibitors, we rescreened all 173 potent molecules for their activity against the schizont-ring transition. In order to obtain specific insights into the inhibitory activity, we employed two levels of validation using flow cytometry and microscopic examination post-inhibitor treatment. Synchronized schizont-stage parasites (40 to 42 hpi) were treated with three different concentrations (1, 3, and 10 μM) of the inhibitors. After 12 h (i.e., at ~55 hpi), the numbers of parasites present as newly formed rings and unruptured schizonts were scored using flow cytometry. Dimethyl sulfoxide (DMSO) and E-64 were included as negative and positive controls, respectively. To observe the

cellular phenotype following inhibitor treatment, microscopic examination of Giemsa-stained smears was performed. We observed that 108 of the 173 molecules showed an inhibitory effect of ≥50% on the [S→R] transition at 10 μM; these numbers dropped to 67 molecules at 3 μM and 32 molecules at 1 μM (Fig. 2B). Although 22 molecules inhibited the [S→R] transition at 1 μM, microscopic analysis of the phenotype indicated that some of them were parasiticidal (and, thus, unlikely to have any direct effect on the egress/invasion process). Molecules inhibiting the [S→R] transition only at 3 μM and 10 μM were not considered for further experiments since at higher concentrations the observed inhibition could have been due to general cytotoxicity on merozoite viability (35, 36).

From these assays, 12 molecules were short-listed as potent and selective [S→R] transition inhibitors at ≤1 μM (Fig. 3A). The following molecules were efficient inhibitors of schizont maturation at submicromolar concentrations: MMV020520, MMV020710, MMV020391, MMV006239, MMV020623, MMV675968, MMV010576, MMV020670, MMV026356, MMV085071, MMV024443, and MMV020081 (Fig. 3B). All inhibitors affecting the schizont-ring transition showed comparable effects against the multidrug-resistant *P. falciparum* Dd2 strain (Fig. 3B). Although parasite release was arrested, these molecules did not appear to hinder merozoite development, as indicated by fluorescence microscopy analysis using the glideosome-associated protein (GAP45) as a marker. GAP45 is phosphorylated by calcium-dependent protein kinase 1 (CDPK1), which is highly active in schizont-stage parasites and regulates cell cycle progression (37–39). In our experiments, a robust signal for GAP45 was detected at the periphery of segmented schizonts (37) (Fig. S3), which indicated the maturation of merozoites in the presence of the molecules. We observed that molecules affecting the schizont-ring transition to some extent affected host cell invasion by merozoites at 3 μM but not at lower concentrations of the drug (Fig. S4).

Microscopy revealed that treatment with MMV020081 and MMV006239 resulted in cellular phenotypes reminiscent of those seen with E-64 treatment, indicating inhibition of egress (Fig. 3C). We then performed a concentration-dependent [S→R] transition assay for the top 12 molecules, as indicated in Fig. 3D. MMV020081 appeared to be the most potent inhibitor with a rupture 50 (R_{50}) value, defined as the concentration of the molecule at which there is a 50% reduction in newly formed rings compared to that for the DMSO control (Table 1). Similarly, MMV024443 showed a substantially higher potency on egress inhibition with an R_{50} value of 0.3 μM, in contrast to its EC_{50} value of 1.65 μM. MMV675968, which was shown to inhibit thymidylate biosynthesis by targeting the dihydrofolate reductase enzyme in *M. tuberculosis* and *T. gondii*, showed comparable values for EC_{50} and R_{50}. All of these molecules belong to diverse chemical classes, indicating that these molecules may act via distinct mechanisms (Fig. S1).

MMV020623, MMV020520, MMV020081, MMV020710, and MMV020391, which are reported to target *P. falciparum* ATP4 (*Pf*ATP4) and disrupt cellular cation homeostasis, were also found to strongly inhibit the [S→R] transition, suggesting a role for *Pf*ATP4 in parasite egress (40, 41). MMV024443 (an indole-2-carboxamide), which has been shown to target *P. falciparum* calcium-dependent protein kinase 1 (*Pf*CDPK1) (42–44), showed excellent egress inhibition in our studies. Previous studies in *P. falciparum* have shown the importance of *Pf*CDPK1 in parasite development and invasion (42–45). Interestingly, we found that this molecule can also inhibit the calcium ionophore-induced egress of *T. gondii* (as discussed below). The *T. gondii* calcium-dependent protein kinase 1 (*Tg*CDPK1) is an essential regulator of calcium-dependent parasite egress and invasion (44). *Pf*CDPK1 and *Tg*CDPK1 are orthologous and share a sequence identity of 53.85%, suggesting that they may have conserved functions in both parasites. We then determined the egress inhibition based on R_{50} estimation (46), which identified 12 molecules with excellent inhibitory potential with submicromolar R_{50} scores.

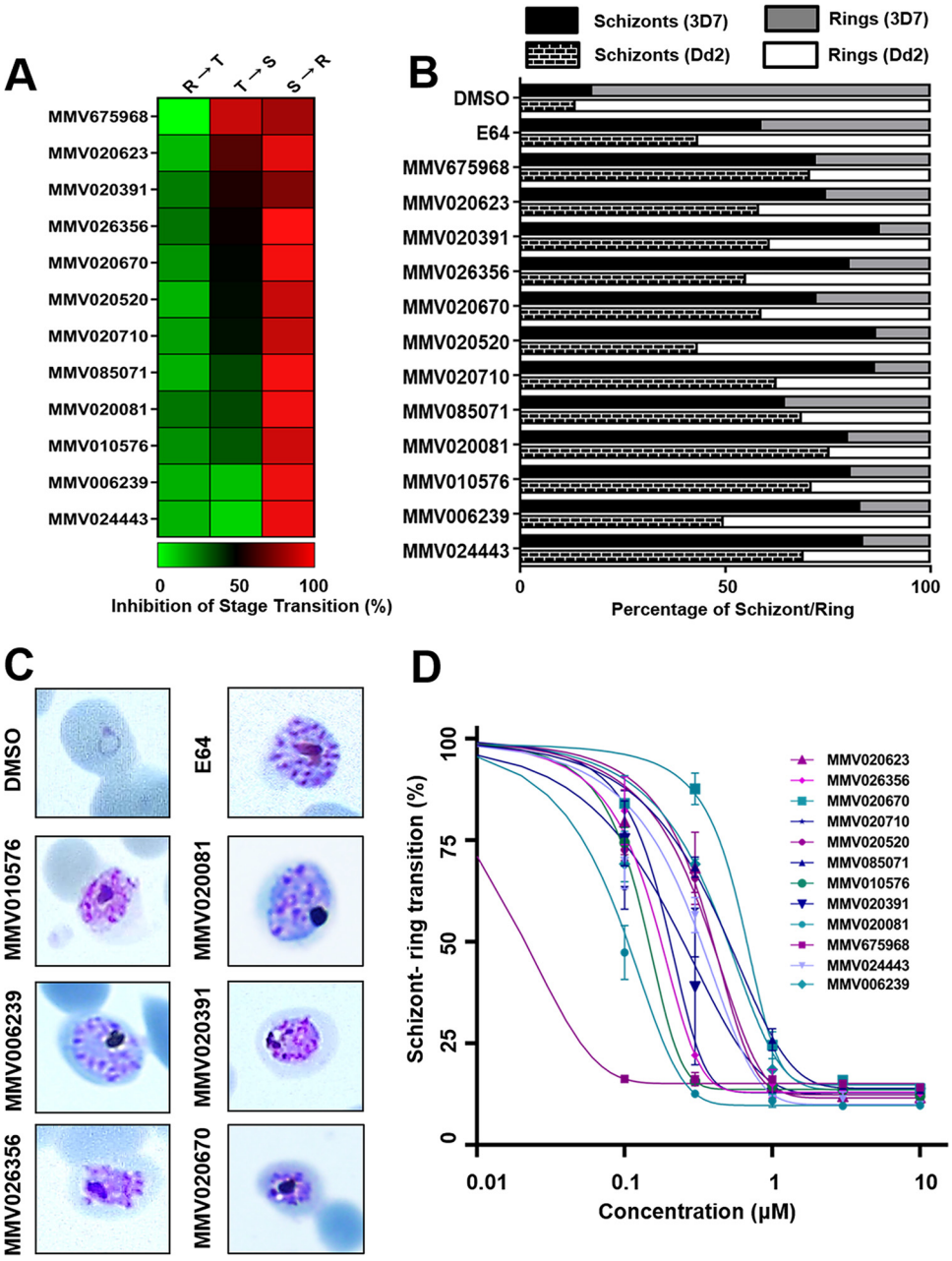

FIG 3 Characterization of schizont inhibitors. (A) (Left) Heat map for 12 potent schizont inhibitors tested at 1 μM for their stage-specific inhibitory effect. While MMV675968 and MMV020623 appeared to affect both trophozoite-to-schizont and schizont-ring transitions, all other molecules were selective against the schizont-ring transition (B) Late-stage schizonts (42 to 44 hpi) incubated with the inhibitors were monitored for inhibition of schizonts of 3D7 and Dd2 parasites through the counting of newly formed rings by flow cytometry. All molecules showed a profound, yet selective activity against the [S→R] transition similar to that of E-64, the positive control for egress inhibition. (C) Giemsa-stained smears upon microscopic investigation revealed the arrest of late-stage parasite development and egress. (D) Dose-response curves indicating inhibition of the schizont-to-ring transition by the most potent schizont inhibitors. DMSO and E-64 were included as negative and positive controls, respectively. The majority of the chosen Pathogen Box molecules showed remarkable schizontocidal activity.

Effect of *Plasmodium* schizont inhibitors on *Toxoplasma* egress. Being an obligate intracellular parasite, *T. gondii* actively invades and proliferates within a parasitophorous vacuole inside host cells. At the end of an intravacuolar replicative cycle (or prematurely in response to perturbations), the parasites egress and reinvade a new host cell in order to continue proliferating. Thus, egress and invasion are the two critical processes which are essential for continuity of the replicative cycle. We were interested

TABLE 1 Top 12 molecules exhibiting late-stage schizont inhibition[a]

Pathogen Box identifier	Chemical class	EC_{50} value (μM)[b]	R_{50} value (μM)[b]	Trophozoite inhibition (%) at 1 μM	Schizont inhibition (%) at 1 μM	DNA damage (%) at 5 μM	*Toxoplasma* ionophore egress time (min) at 10 μM[d]	Function and possible targets [reference(s)]
MMV024443	Indole derivatives	1.66	0.306	NA[c]	58.6	30	7.00	CDPK1 (calcium-dependent protein kinase 1) lactate dehydrogenase (39–41)
MMV020623	Indole derivatives	0.22	0.414	14.15	70.6	30–40	4.10	*Pf*ATP4 dysregulation affecting Na+ efflux (41)
MMV010576	Pyridine and derivatives	0.19	0.138	20.57	60.4	30	6.50	Phosphatidylinositol 4-kinase (PI4K) activity (8), based on the elucidated target for clinical candidate MMV390048
MMV020520	Benzoxazines	0.22	0.432	35.84	84.6	30	3.30	*Pf*ATP4 dysregulation affecting Na^+ efflux (41)
MMV085071	Indole derivatives	0.03	0.470	36.89	47.2	30	6.50	Rapid parasiticidal effect and programmed cell death (PCD)-like phenotypes (12)
MMV020670	6-Naphthyridine-2-carboxamide	1.56	0.787	37.03	64	>50	7.00	NA
MMV020081	Benzene and substituted derivatives	0.07	0.089	38.23	43.4	30	7.00	*Pf*ATP4 dysregulation affecting Na^+ efflux (41)
MMV026356	2-Methylpyrazole-3-carboxamide	1.70	0.156	40.27	61.4	>50	7.00	NA
MMV006239	Alkaloid derivatives	0.16	0.495	42.32	90	25–30	7.00	NA
MMV020710	Azoles	0.06	0.241	43.63	84	25–30	7.00	*Pf*ATP4 dysregulation affecting Na^+ efflux (41)
MMV020391	Benzene and substituted derivatives	0.11	0.132	44.04	90.4	25–30	NA	*Pf*ATP4 dysregulation affecting Na^+ efflux (41)
MMV675968	Diazanaphthalenes	0.07	0.083	77.48	41.6	25–30	NA	Inhibits dihydrofolate reductase (*Toxoplasma* and *Cryptosporidium*) (11)

[a]The table lists 12 schizont inhibitors, their chemical class, consolidated study results, and their predicted mechanism of action.
[b]Data are from this study
[c]NA, not available.
[d]Egress was monitored up to a maximum of 7 min.

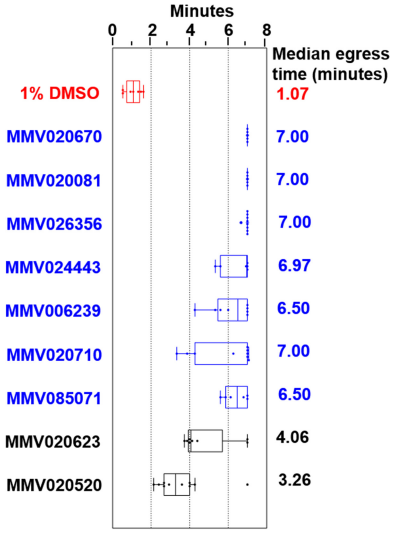

FIG 4 *P. falciparum* [S→R] transition blockers inhibit the calcium ionophore-mediated egress of *T. gondii* tachyzoites. Whisker plots show the timing of ionophore-induced egress following 24 h of treatment for Pathogen Box molecules at 10 μM. Red, 1% DMSO-treated control cells; blue, inhibitors for which the median egress time was >6 min.

in finding out whether any of the Pathogen Box molecules which affected the egress of *P. falciparum* merozoites might inhibit the egress of tachyzoite-stage *T. gondii*. For this, we used a calcium ionophore-mediated egress assay as previously reported (47). Intracellular tachyzoite-stage parasites were treated with 10 μM of the chosen inhibitors for 24 h, following which egress was induced using a calcium ionophore (A23187). DMSO (1%)-treated parasites were kept as controls to determine the time taken for normal parasite release. Of the 12 molecules tested, 9 were capable of inhibiting *T. gondii* egress from host cells. The average egress time for DMSO-treated parasites was ~1.07 min. For inhibitor-treated parasites, we considered an average egress time delay of at least 4 min to assign them as potential egress inhibitors of *T. gondii* (Fig. 4A). Interestingly, we identified 7 molecules (MMV020081, MMV085071, MMV024443, MMV026356, MMV020670, MMV006239, and MMV020710) with significant egress-blocking activity, and at least in the case of 3 molecules (MMV020670, MMV020081, and MMV026356), the egress block extended beyond 7 min (Fig. 4A; the results for the 7 molecules with significant egress-blocking activity are highlighted in blue). Only MMV020623 (average egress time, ~4.06 min) and MMV020520 (average egress time, ~3.26 min) showed modest inhibition of *T. gondii* egress.

Mechanistic insights into the action of MMV020391 and MMV010576. Although we identified several molecules with inhibitory potential against schizont-ring transition and egress, it is reasonable to expect that these molecules have different targets and operate differently at the molecular level, given their structural diversity. Furthermore, microscopy of cellular phenotypes revealed both an apparent egress inhibition phenotype (MMV020391 and MMV010576) and less distinct ones (MMV026356 and MMV020670). Molecules that are cytotoxic could kill parasites by producing reactive oxygen species (ROS), thus damaging parasite proteins and DNA (40, 48). To validate such a possibility, we evaluated ROS generation in late-stage schizonts treated with the 7 molecules that were effective against both *Plasmodium* and *Toxoplasma* (MMV020081, MMV085071, MMV024443, MMV026356, MMV020670, MMV006239, and MMV020710). All 7 molecules were positive for ROS generation, albeit to various degrees (Fig. 5A). Following this observation, we performed a quantitative flow cytometry-based ROS assay, which indicated that at least 5 of these molecules (MMV006239, MMV020670, MMV026356, MMV024443, and MMV085071) were potent ROS generators (Fig. 5B).

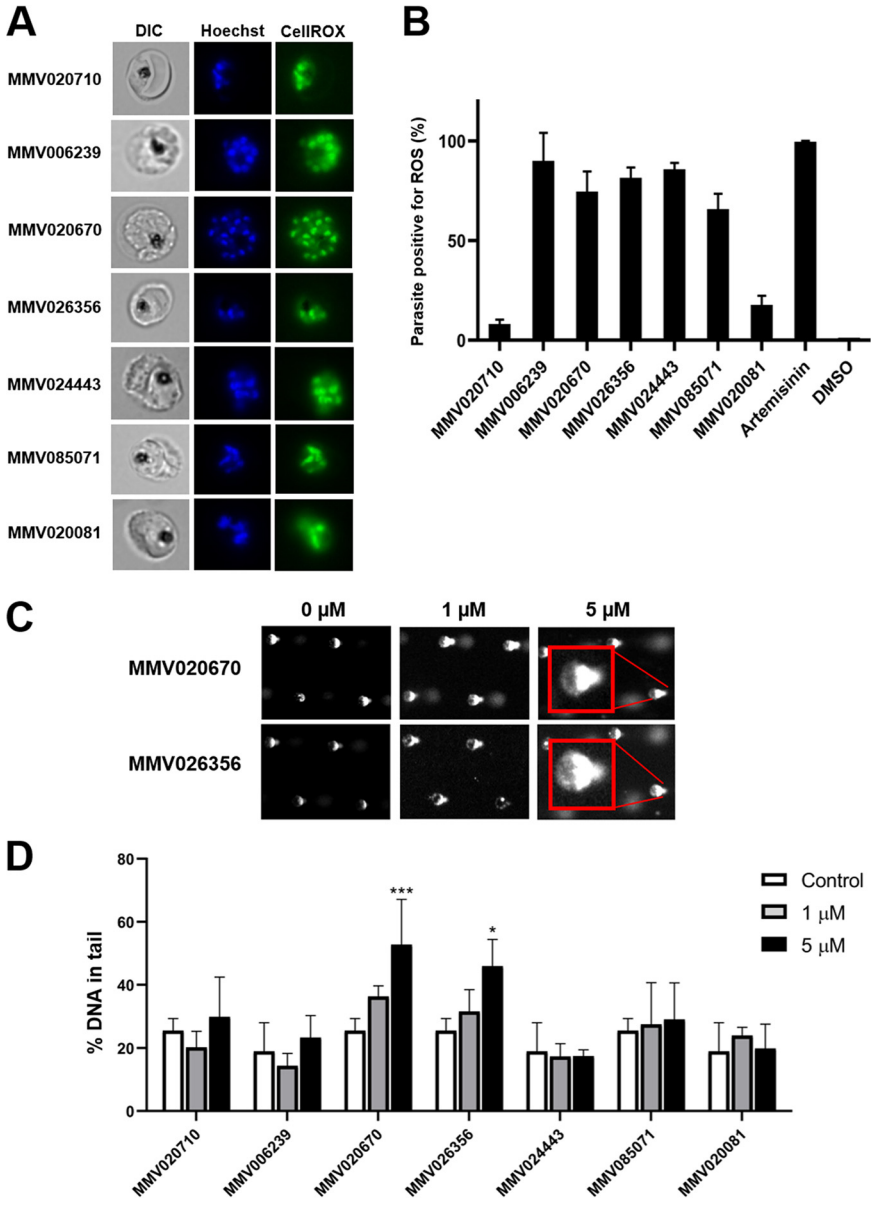

FIG 5 ROS production and DNA fragmentation by Pathogen Box molecules that inhibit parasite egress. (A) Evaluation of ROS production visualized by staining with CellROX green after 3 h of treatment with 1 μM and 5 μM the chosen inhibitors. Various degrees of ROS production are evident from the observed green fluorescence. (B) Quantification of ROS production using flow cytometry revealed a high extent of ROS production upon treatment with MMV020670, MMV026356, and MMV024443. (C and D) Results from the comet assay showing DNA damage in late-stage parasites treated with MMV020670 and MMV026356. None of the other molecules showed detectable DNA fragmentation.

Since increased intracellular ROS can cause DNA damage, we used a comet assay to visualize the extent of DNA damage/breakdown following inhibitor treatment. From these experiments, $\geq$50% DNA damage was observed following treatment with MMV020670 and MMV026356 (Fig. 5C), as indicated by comet tail moment at 5 μM drug exposure (Fig. 5D). Thus, it is likely that the increased level of ROS in MMV020670- and MMV026356-treated parasites may be responsible for the observed DNA damage. A variety of cellular mechanisms can enable ROS production, including oxidation of lipids, protein, and other cellular regulatory mechanisms (49–51).

Targeting the [S→R] transition offers an excellent opportunity for the development of chemotherapy against *Plasmodium* infection. First, by blocking newly formed

invasion-ready merozoites from egressing out of infected RBCs, a rapid increase in the parasite load can be prevented. Second, the [S→R] transition involves preparatory remodeling events in the parasite, which offer numerous targets for inhibitors. Further mechanistic studies on the Pathogen Box molecules identified in this study as [S→R] transition inhibitors are needed to fully realize the therapeutic potential of these molecules. Studies on altered gene and protein expression, combined with proteome modification studies, can be good starting points for obtaining further insights into the mechanism of these molecules.

Conclusions. Growth inhibition studies against blood-stage *P. falciparum* using the MMV Pathogen Box library identified 173 antimalarial molecules, of which 72 molecules are newly identified. Further, we segregated these molecules based on stage selectivity, inhibitory efficacy, and cellular phenotypes, which allowed us to prioritize 12 molecules that interfere with late-stage parasite development and egress. We demonstrate that two of the schizont inhibitors, MMV020670 and MMV026356, induce DNA breakdown in segmented schizonts, leading to parasite arrest. Identifying molecules that inhibit egress in both *Plasmodium and Toxoplasma* is exciting, as this can facilitate target identification and mechanism studies. This also opens up the possibility of exploiting these molecules as therapeutic agents with activity against multiple apicomplexan parasites.

MATERIALS AND METHODS

Ethics statement. All experiments were conducted in accordance with the approved guidelines of the Singapore University of Technology and Design (SUTD).

Pathogen Box chemical library: stock solutions and storage. The MMV Pathogen Box was received in 96-well plates as 10 mM stocks in 100% dimethyl sulfoxide (DMSO). The stocks were diluted and aliquoted to 5 subsets with a final drug concentration of 1 mM in DMSO (20 μl of stock solution and 180 μl of filtered DMSO), as recommended by MMV. These plates were stored at −80°C. Care was taken to avoid multiple freeze-thaw cycles of the plates during the course of this study.

***P. falciparum in vitro* culturing, synchronization, and maintenance.** Blood for culturing of *P. falciparum* was purchased from Interstate Blood Bank (USA). All experiments reported in this study used the 3D7 strain of *P. falciparum*, and infected RBCs were maintained in sodium bicarbonate–HEPES-buffered RPMI 1640 culture medium (Sigma-Aldrich, Singapore), at pH 7.4, supplemented with hypoxanthine and 2.5 mg/ml AlbuMAX II lipid-rich bovine serum albumin (BSA) (Gibco). Ring-stage parasites were synchronized by treatment with 5% sorbitol at 37°C. The parasites used for the schizont-ring transition assays were enriched using separation by magnetic-activated cell sorting (MACS; Miltenyi Biotech, Bergisch Gladbach, Germany), as reported in prior work (52). Parasitemia was scored using flow cytometry (Accuri C6 sampler; BD Biosciences, Singapore) after the paraformaldehyde-fixed parasites were stained with Hoechst (Hoechst 33342; Thermo Fisher Scientific, Inc.). In parallel, Giemsa-stained smears were microscopically examined to match the smear findings with the flow cytometry results and to record the phenotypic characteristics arising from drug treatment, as established previously (46, 53).

EC_{50} determination of Pathogen Box molecules against *P. falciparum*. Antimalarial efficacy screening was performed in a 96-well plate format. The molecules were plated by 2-fold serial dilution from 10 μM to 0.01 μM, and the parasite culture (200 μl per well) was introduced at 2.5% hematocrit and an ~2% starting parasitemia. As positive controls, the antimalarial drugs atovaquone and/or chloroquine were used at 1 μM each, while 1% DMSO served as the negative control. The parasites were allowed to grow for 60 h under optimal growth conditions. For assay readout, 25 μl of staining reagent (10× SYBR green and 0.5% Triton X-100 in phosphate-buffered saline [PBS], pH 7.4) was mixed into each well. The fluorescence emitted by DNA-bound dye was quantified, using excitation and emission wavelengths of 498 nm and 522 nm, respectively, in a GloMax plate reader (Promega). Data processing and statistical analysis were performed using Microsoft Excel software.

Stage transition inhibition assay. The 90 most potent molecules ($EC_{50} \leq 1$ μM) were chosen for testing of their stage-specific inhibitory effect during *P. falciparum* development. A stage transition (ring to trophozoite) assay was performed by incubating ring-stage parasites (4 to 6 hpi, 4% parasitemia) with molecules for 24 h until trophozoites appeared in the DMSO-treated controls. Trophozoite-to-schizont transition inhibition was estimated by treating parasites (24 to 26 hpi, 4% parasitemia) for 12 h until early schizonts (36 to 38 hpi) appeared in the DMSO-treated controls. For schizont-to-ring inhibition, parasites (40 to 42 hpi, 4% parasitemia) were treated with molecules for 20 h until ring-stage parasites appeared in the DMSO-treated controls. In all cases, samples were fixed with 0.1% glutaraldehyde–PBS overnight, and flow cytometry was performed on an Accuri C6 instrument (BD Biosciences). For each treatment replicate, 100,000 events were recorded. Statistical analysis was performed using GraphPad Prism software (46, 54).

For determining the R_{50} value, schizont-stage parasites (~40 to 42 hpi) were treated with the inhibitors at 10, 3, 1, 0.3, and 0.1 μM for 12 h. When ring-stage parasites were observed in the DMSO-treated controls, cells were harvested for flow cytometry analysis, followed by estimation of

the R_{50}, as described in prior work (46). E-64, a known inhibitor of *P. falciparum* egress, was used as a positive control (55).

Measurement of intracellular ROS. Magnet-purified schizont-stage parasites (~42 to 44 hpi) were treated with selected molecules at a concentration of 1 μM for 1 h. Following incubation, 5 μM CellROX green reagent (Thermo Fisher Scientific, Inc.) was added to the cells, and the cells were incubated for 30 min in a 5% CO_2 incubator at 37°C. The cells were costained with Hoechst 33342 during the last 15 min of incubation in malaria culture medium (MCM) at 37°C in the dark. The cells were then washed with PBS three times and visualized using a fluorescence microscope (Olympus CKX53 inverted microscope).

Assessment of DNA damage using a CometChip. An alkaline CometChip assay was performed as described previously (56, 57). Briefly, schizont-stage *P. falciparum* parasites were enriched on a Percoll gradient and resuspended in complete RPMI at 0.5% (vol/vol). Cell suspensions were incubated with different concentrations of drugs or mock solution (0.05% DMSO) in a 96-well plate for 1 h at 37°C. Treated cells were transferred to a CometChip, lysed overnight at 4°C in alkaline lysis buffer, and subjected to electrophoresis at 4°C for 30 min at 1 V/cm and ~300 mA with alkaline electrophoresis buffer as previously described (56). The chip was then washed twice at room temperature with a neutralization buffer containing 0.4 M Trizma HCl (Sigma-Aldrich, USA). The CometChip was stained with 1× SYBR gold (Invitrogen, USA) for 30 min at room temperature in the dark. Fluorescent images of the comets were captured at a ×40 magnification using an epifluorescence microscope (Olympus IX83) with a 480-nm excitation filter. Images were analyzed using Guicometanalyzer, customized software developed in MATLAB (The MathWorks Inc., USA), as previously described (57). The median number of comets in each well was calculated from results generated in Guicometanalyzer and converted into an Excel file using Comet to Excel, a program developed in Python.

Egress inhibition studies in *Toxoplasma gondii*. Tachyzoite-stage RH strain *T. gondii* parasites were cultured in the laboratory as previously reported (53). When exposed to the calcium ionophore A23187, intracellular tachyzoites are known to rapidly rupture the parasitophorous vacuole and egress out of the host cells (47, 58, 59). Here, the ionophore-induced egress of *T. gondii* tachyzoites was performed after treating the parasites with selected inhibitors (at 10 μM for 24 h) to assess their effect on the egress process. The time that elapsed after addition of the ionophore for vacuole rupture and parasite egress was monitored by time-lapse microscopy using a 40× objective fitted to an inverted bright-field microscope (Primo Vert; Zeiss). Images were captured at 30-s intervals for a 10-min period.

Merozoite invasion assay. Synchronized late-stage schizonts were isolated by use of a MACS magnetic column (Miltenyi Biotech). Purified (>95%) schizonts were washed twice in MCM and incubated for 6 to 8 h with 10 μM E-64 to get completely mature segmented schizonts, as reported previously (60). Schizonts were pelleted at 2,200 rpm for 3 min and washed twice in RPMI. The parasites were resuspended in 5 ml MCM at room temperature and filtered through a 2-μm-pore-size-disc 25-mm syringe filter. Merozoites were collected by centrifugation, suspended by pipetting gently, and introduced into wells containing RBCs and the desired concentration of the drugs along with positive controls for invasion inhibition, such as cytochalasin B and heparin. The 96-well plate was immediately placed inside a Ziplock bag, gassed, and incubated at 37°C with shaking for 2 h. The culture was then placed under normal growth conditions for 16 h, after which parasitemia was scored by flow cytometry. Giemsa-stained smears were prepared in parallel for microscopic validation.

Immunofluorescence microscopy to analyze merozoite maturation. Schizont-stage parasites (~44 hpi) were treated with egress-inhibitory molecules at 1 μM along with the DMSO-treated controls. At the time when late-stage rings were present in the control culture, egress-inhibited infected RBCs from drug-treated wells were transferred to glass slides. These samples were then fixed with 4% paraformaldehyde and permeabilized with 0.1% (vol/vol) Tween 20 in 1× PBS. After blocking with 3% (wt/vol) BSA in 1× PBS for 1 h, samples were incubated with anti-*Pf*GAP45 antibody (1:2,000) in blocking buffer for 1 h at 37°C, followed by two washes with 1× PBS (37, 38). Samples were then incubated for 45 min at room temperature with appropriate secondary antibody conjugated with Alexa Fluor 488 (Life Technologies). The slides were mounted for microscopic examination using an antifade reagent with DAPI (4′,6-diamidino-2-phenylindole; Life Technologies). Images from the fluorescence microscope were analyzed using ImageJ software and prepared for publication with Adobe Photoshop. Trophozoite-stage parasites were used as a negative control for *Pf*GAP45 staining.

SUPPLEMENTAL MATERIAL

Supplemental material is available online only.

SUPPLEMENTAL FILE 1, PDF file, 0.7 MB.

SUPPLEMENTAL FILE 2, XLS file, 4.5 MB.

ACKNOWLEDGMENTS

We thank MMV for providing the Pathogen Box chemical library used in this research. We also thank Anthony A. Holder (Francis Crick Institute, London, United Kingdom) for the gift to us of the recombinant *Pf*GAP45 antibody. Thanks go to Kevin S. Tan (National University of Singapore), D. S. Reddy (CSIR-National Chemical Laboratories, India), Omar Sheriff, and Prem Prakash (Nanyang Technological University) for various discussions.

A.T.P., G.S., and R.C. acknowledge the following grants: RGAST1503 (A*star-India

Collaboration grant) and T1MOE1702 (a Ministry of Education [MoE] Tier 1 grant awarded through SUTD). A.T.P. acknowledges the MoE, Singapore, for a president's graduate fellowship. The infrastructure support provided through the SUTD-MIT International Design Centre (IDC) is greatly acknowledged. M.A.B. and T.H. acknowledge Ph.D. fellowships from the Council of Scientific and Industrial Research, India; D.S. acknowledges the Indo-Singapore Joint Science and Technology Research Cooperation grant from the Department of Science and Technology, India (grant INT/SIN/P-09/2015), and infrastructure support from the CSIR-National Chemical Laboratory, Pune, India.

The funders had no role in study design, data collection and interpretation, or the decision to submit the work for publication.

A.T.P. was involved in study design, conducted *Plasmodium* experiments, analyzed results, prepared figures, and assisted with manuscript preparation; T.H. performed antimalarial screening for all Pathogen Box molecules, analyzed results, and assisted with manuscript preparation; M.A.B. performed *T. gondii* egress assays and analyzed results; A.X. performed the comet assay, analyzed results, and assisted with manuscript preparation; G.S. assisted with *Plasmodium* experiments and assisted with manuscript preparation; Z.B. was involved in study design, provided tools/reagents, and assisted with manuscript preparation; P.P. was involved in study design, provided tools/reagents, and assisted with manuscript preparation; D.S. was involved in study design, analyzed data, verified results, and assisted with manuscript preparation; and R.C. designed the study, coordinated the research, verified results, and wrote the manuscript.

We have no conflicts of interest to declare.

REFERENCES

1. Ashburn TT, Thor KB. 2004. Drug repositioning: identifying and developing new uses for existing drugs. Nat Rev Drug Discov 3:673–683. https://doi.org/10.1038/nrd1468.
2. Scannell JW, Blanckley A, Boldon H, Warrington B. 2012. Diagnosing the decline in pharmaceutical R&D efficiency. Nat Rev Drug Discov 11:191–200. https://doi.org/10.1038/nrd3681.
3. Black MW, Arrizabalaga G, Boothroyd JC. 2000. Ionophore-resistant mutants of Toxoplasma gondii reveal host cell permeabilization as an early event in egress. Mol Cell Biol 20:9399–9408. https://doi.org/10.1128/mcb.20.24.9399-9408.2000.
4. Van Voorhis WC, Adams JH, Adelfio R, Ahyong V, Akabas MH, Alano P, Alday A, Alemán Resto Y, Alsibaee A, Alzualde A, Andrews KT, Avery SV, Avery VM, Ayong L, Baker M, Baker S, Ben Mamoun C, Bhatia S, Bickle Q, Bounaadja L, Bowling T, Bosch J, Boucher LE, Boyom FF, Brea J, Brennan M, Burton A, Caffrey CR, Camarda G, Carrasquilla M, Carter D, Belen Cassera M, Chih-Chien Cheng K, Chindaudomsate W, Chubb A, Colon BL, Colón-López DD, Corbett Y, Crowther GJ, Cowan N, D'Alessandro S, Le Dang N, Delves M, DeRisi JL, Du AY, Duffy S, Abd El-Salam El-Sayed S, Ferdig MT, Fernández Robledo JA, Fidock DA, et al. 2016. Open source drug discovery with the Malaria Box compound collection for neglected diseases and beyond. PLoS Pathog 12:e1005763. https://doi.org/10.1371/journal.ppat.1005763.
5. Preston S, Jiao Y, Jabbar A, McGee SL, Laleu B, Willis P, Wells TNC, Gasser RB. 2016. Screening of the 'Pathogen Box' identifies an approved pesticide with major anthelmintic activity against the barber's pole worm. Int J Parasitol Drugs Drug Resist 6:329–334. https://doi.org/10.1016/j.ijpddr.2016.07.004.
6. Vila T, Lopez-Ribot JL. 2017. Screening the Pathogen Box for identification of Candida albicans biofilm inhibitors. Antimicrob Agents Chemother 61:e02006-16. https://doi.org/10.1128/AAC.02006-16.
7. Mansour NR, Paveley R, Gardner JM, Bell AS, Parkinson T, Bickle Q. 2016. High throughput screening identifies novel lead compounds with activity against larval, juvenile and adult Schistosoma mansoni. PLoS Negl Trop Dis 10:e0004659. https://doi.org/10.1371/journal.pntd.0004659.
8. Hennessey KM, Rogiers IC, Shih HW, Hulverson MA, Choi R, McCloskey MC, Whitman GR, Barrett LK, Merritt EA, Paredez AR, Ojo KK. 2018. Screening of the Pathogen Box for inhibitors with dual efficacy against Giardia lamblia and Cryptosporidium parvum. PLoS Negl Trop Dis 12:e0006673. https://doi.org/10.1371/journal.pntd.0006673.
9. Rufener R, Dick L, D'Ascoli L, Ritler D, Hizem A, Wells TNC, Hemphill A, Lundström-Stadelmann B. 2018. Repurposing of an old drug: in vitro and in vivo efficacies of buparvaquone against Echinococcus multilocularis. Int J Parasitol Drugs Drug Resist 8:440–450. https://doi.org/10.1016/j.ijpddr.2018.10.011.
10. Duffy S, Sykes ML, Jones AJ, Shelper TB, Simpson M, Lang R, Poulsen SA, Sleebs BE, Avery VM. 2017. Screening the Medicines for Malaria Venture Pathogen Box across multiple pathogens reclassifies starting points for open-source drug discovery. Antimicrob Agents Chemother 61:e00379-17. https://doi.org/10.1128/AAC.00379-17.
11. Spalenka J, Escotte-Binet S, Bakiri A, Hubert J, Renault JH, Velard F, Duchateau S, Aubert D, Huguenin A, Villena I. 2018. Discovery of new inhibitors of Toxoplasma gondii via the Pathogen Box. Antimicrob Agents Chemother 62:e01640-17. https://doi.org/10.1128/AAC.01640-17.
12. Tong JX, Chandramohanadas R, Tan KS. 2018. High-content screening of the Medicines for Malaria Venture Pathogen Box for Plasmodium falciparum digestive vacuole-disrupting molecules reveals valuable starting points for drug discovery. Antimicrob Agents Chemother 62:e02031-17. https://doi.org/10.1128/AAC.02031-17.
13. Cibulskis RE, Alonso P, Aponte J, Aregawi M, Barrette A, Bergeron L, Fergus CA, Knox T, Lynch M, Patouillard E, Schwarte S, Stewart S, Williams R. 2016. Malaria: global progress 2000–2015 and future challenges. Infect Dis Poverty 5:61. https://doi.org/10.1186/s40249-016-0151-8.
14. Doumbo O, Fall IS, Niare D. 2016. Malaria is still a leading cause of fever and death among children and pregnant women in Africa in 2015. Bull Acad Natl Med 200:453–466. (In French.)
15. Chitnis CE, Staines HM. 2013. Dealing with change: the different microenvironments faced by the malarial parasite. Mol Microbiol 88:1–4. https://doi.org/10.1111/mmi.12179.
16. Bhatnagar S, Nicklas S, Morrisey JM, Goldberg DE, Vaidya AB. 2019. Diverse chemical compounds target Plasmodium falciparum plasma membrane lipid homeostasis. ACS Infect Dis 5:550–558. https://doi.org/10.1021/acsinfecdis.8b00277.
17. Calit J, Dobrescu I, Gaitan XA, Borges MH, Ramos MS, Eastman RT, Bargieri DY. 2018. Screening the Pathogen Box for molecules active against Plasmodium sexual stages using a new nanoluciferase-based transgenic line of P. berghei identifies transmission-blocking compounds. Antimicrob Agents Chemother 62:e01053-18. https://doi.org/10.1128/AAC.01053-18.

18. Bakunov SA, Bakunova SM, Wenzler T, Barszcz T, Werbovetz KA, Brun R, Tidwell RR. 2008. Synthesis and antiprotozoal activity of cationic 2-phenylbenzofurans. J Med Chem 51:6927–6944. https://doi.org/10.1021/jm800918v.
19. Stephens CE, Brun R, Salem MM, Werbovetz KA, Tanious F, Wilson WD, Boykin DW. 2003. The activity of diguanidino and 'reversed' diamidino 2,5-diarylfurans versus Trypanosoma cruzi and Leishmania donovani. Bioorg Med Chem Lett 13:2065–2069. https://doi.org/10.1016/s0960-894x(03)00319-6.
20. Rodriguez F, Rozas I, Kaiser M, Brun R, Nguyen B, Wilson WD, Garcia RN, Dardonville C. 2008. New bis(2-aminoimidazoline) and bisguanidine DNA minor groove binders with potent in vivo antitrypanosomal and antiplasmodial activity. J Med Chem 51:909–923. https://doi.org/10.1021/jm7013088.
21. Tatipaka HB, Gillespie JR, Chatterjee AK, Norcross NR, Hulverson MA, Ranade RM, Nagendar P, Creason SA, McQueen J, Duster NA, Nagle A, Supek F, Molteni V, Wenzler T, Brun R, Glynne R, Buckner FS, Gelb MH. 2014. Substituted 2-phenylimidazopyridines: a new class of drug leads for human African trypanosomiasis. J Med Chem 57:828–835. https://doi.org/10.1021/jm401178t.
22. Yuthavong Y, Yuvaniyama J, Chitnumsub P, Vanichtanankul J, Chusacultanachai S, Tarnchompoo B, Vilaivan T, Kamchonwongpaisan S. 2005. Malarial (Plasmodium falciparum) dihydrofolate reductase-thymidylate synthase: structural basis for antifolate resistance and development of effective inhibitors. Parasitology 130:249–259. https://doi.org/10.1017/s003118200400664x.
23. Fan YL, Cheng XW, Wu JB, Liu M, Zhang FZ, Xu Z, Feng LS. 2018. Antiplasmodial and antimalarial activities of quinolone derivatives: an overview. Eur J Med Chem 146:1–14. https://doi.org/10.1016/j.ejmech.2018.01.039.
24. Shiro T, Fukaya T, Tobe M. 2015. The chemistry and biological activity of heterocycle-fused quinolinone derivatives: a review. Eur J Med Chem 97:397–408. https://doi.org/10.1016/j.ejmech.2014.12.004.
25. Ballell L, Bates RH, Young RJ, Alvarez-Gomez D, Alvarez-Ruiz E, Barroso V, Blanco D, Crespo B, Escribano J, González R, Lozano S, Huss S, Santos-Villarejo A, Martín-Plaza JJ, Mendoza A, Rebollo-Lopez MJ, Remuiñan-Blanco M, Lavandera JL, Pérez-Herran E, Gamo-Benito FJ, García-Bustos JF, Barros D, Castro JP, Cammack N. 2013. Fueling open-source drug discovery: 177 small-molecule leads against tuberculosis. ChemMedChem 8:313–321. https://doi.org/10.1002/cmdc.201200428.
26. Aquino CJ, Ramanjulu JM, Heyer D, Daniels AJ, Palazzo F, Dezube M. 2004. Synthesis and structure activity relationship of guanidines as NPY Y5 antagonists. Bioorg Med Chem 12:2691–2708. https://doi.org/10.1016/j.bmc.2004.03.012.
27. Hodel EM, Kay K, Hastings IM. 2016. Incorporating stage-specific drug action into pharmacological modeling of antimalarial drug treatment. Antimicrob Agents Chemother 60:2747–2756. https://doi.org/10.1128/AAC.01172-15.
28. Kerlin DH, Boyce K, Marfurt J, Simpson JA, Kenangalem E, Cheng Q, Price RN, Gatton ML. 2012. An analytical method for assessing stage-specific drug activity in Plasmodium vivax malaria: implications for ex vivo drug susceptibility testing. PLoS Negl Trop Dis 6:e1772. https://doi.org/10.1371/journal.pntd.0001772.
29. Klonis N, Xie SC, McCaw JM, Crespo-Ortiz MP, Zaloumis SG, Simpson JA, Tilley L. 2013. Altered temporal response of malaria parasites determines differential sensitivity to artemisinin. Proc Natl Acad Sci U S A 110:5157–5162. https://doi.org/10.1073/pnas.1217452110.
30. Wilson DW, Langer C, Goodman CD, McFadden GI, Beeson JG. 2013. Defining the timing of action of antimalarial drugs against Plasmodium falciparum. Antimicrob Agents Chemother 57:1455–1467. https://doi.org/10.1128/AAC.01881-12.
31. Painter HJ, Morrisey JM, Vaidya AB. 2010. Mitochondrial electron transport inhibition and viability of intraerythrocytic Plasmodium falciparum. Antimicrob Agents Chemother 54:5281–5287. https://doi.org/10.1128/AAC.00937-10.
32. Zhang Y, Asante KS, Jung A. 1986. Stage-dependent inhibition of chloroquine on Plasmodium falciparum in vitro. J Parasitol 72:830–836. https://doi.org/10.2307/3281830.
33. Beteck RM, Seldon R, Jordaan A, Warner DF, Hoppe HC, Laming D, Khanye SD. 2019. New quinolone-based thiosemicarbazones showing activity against Plasmodium falciparum and Mycobacterium tuberculosis. Molecules 24:E1740. https://doi.org/10.3390/molecules24091740.
34. Veale C. 2019. Unpacking the Pathogen Box—an open source tool for fighting neglected tropical disease. ChemMedChem 14:386–453. https://doi.org/10.1002/cmdc.201800755.
35. Happi GM, Kouam SF, Talontsi FM, Lamshoft M, Zuhlke S, Bauer JO, Strohmann C, Spiteller M. 2015. Antiplasmodial and cytotoxic triterpenoids from the bark of the Cameroonian medicinal plant Entandrophragma congoense. J Nat Prod 78:604–614. https://doi.org/10.1021/np5004164.
36. Elloumi-Mseddi J, Msalbi D, Fakhfakh R, Aifa S. 2019. Anti-diarrheal drug repositioning in tumour cell cytotoxicity. Anticancer Agents Med Chem 19:1037–1047. https://doi.org/10.2174/1871520619666190118120030.
37. Rees-Channer RR, Martin SR, Green JL, Bowyer PW, Grainger M, Molloy JE, Holder AA. 2006. Dual acylation of the 45 kDa gliding-associated protein (GAP45) in Plasmodium falciparum merozoites. Mol Biochem Parasitol 149:113–116. https://doi.org/10.1016/j.molbiopara.2006.04.008.
38. Ridzuan MA, Moon RW, Knuepfer E, Black S, Holder AA, Green JL. 2012. Subcellular location, phosphorylation and assembly into the motor complex of GAP45 during Plasmodium falciparum schizont development. PLoS One 7:e33845. https://doi.org/10.1371/journal.pone.0033845.
39. Green JL, Rees-Channer RR, Howell SA, Martin SR, Knuepfer E, Taylor HM, Grainger M, Holder AA. 2008. The motor complex of Plasmodium falciparum: phosphorylation by a calcium-dependent protein kinase. J Biol Chem 283:30980–30989. https://doi.org/10.1074/jbc.M803129200.
40. Dennis ASM, Rosling JEO, Lehane AM, Kirk K. 2018. Diverse antimalarials from whole-cell phenotypic screens disrupt malaria parasite ion and volume homeostasis. Sci Rep 8:8795. https://doi.org/10.1038/s41598-018-26819-1.
41. Spillman NJ, Allen RJ, McNamara CW, Yeung BK, Winzeler EA, Diagana TT, Kirk K. 2013. Na(+) regulation in the malaria parasite Plasmodium falciparum involves the cation ATPase PfATP4 and is a target of the spiroindolone antimalarials. Cell Host Microbe 13:227–237. https://doi.org/10.1016/j.chom.2012.12.006.
42. Ansell KH, Jones HM, Whalley D, Hearn A, Taylor DL, Patin EC, Chapman TM, Osborne SA, Wallace C, Birchall K, Large J, Bouloc N, Smiljanic-Hurley E, Clough B, Moon RW, Green JL, Holder AA. 2014. Biochemical and antiparasitic properties of inhibitors of the Plasmodium falciparum calcium-dependent protein kinase PfCDPK1. Antimicrob Agents Chemother 58:6032–6043. https://doi.org/10.1128/AAC.02959-14.
43. Bansal A, Singh S, More KR, Hans D, Nangalia K, Yogavel M, Sharma A, Chitnis CE. 2013. Characterization of Plasmodium falciparum calcium-dependent protein kinase 1 (PfCDPK1) and its role in microneme secretion during erythrocyte invasion. J Biol Chem 288:1590–1602. https://doi.org/10.1074/jbc.M112.411934.
44. Lourido S, Tang K, Sibley LD. 2012. Distinct signalling pathways control Toxoplasma egress and host-cell invasion. EMBO J 31:4524–4534. https://doi.org/10.1038/emboj.2012.299.
45. Kumar S, Kumar M, Ekka R, Dvorin JD, Paul AS, Madugundu AK, Gilberger T, Gowda H, Duraisingh MT, Keshava Prasad TS, Sharma P. 2017. PfCDPK1 mediated signaling in erythrocytic stages of Plasmodium falciparum. Nat Commun 8:63. https://doi.org/10.1038/s41467-017-00053-1.
46. Subramanian G, Belekar MA, Shukla A, Tong JX, Sinha A, Chu TTT, Kulkarni AS, Preiser PR, Reddy DS, Tan KSW, Shanmugam D, Chandramohanadas R. 2018. Targeted phenotypic screening in Plasmodium falciparum and Toxoplasma gondii reveals novel modes of action of Medicines for Malaria Venture Malaria Box molecules. mSphere 3:e00534-17. https://doi.org/10.1128/mSphere.00534-17.
47. Endo T, Sethi KK, Piekarski G. 1982. Toxoplasma gondii: calcium ionophore A23187-mediated exit of trophozoites from infected murine macrophages. Exp Parasitol 53:179–188. https://doi.org/10.1016/0014-4894(82)90059-5.
48. Salehi F, Behboudi H, Kavoosi G, Ardestani SK. 2018. Oxidative DNA damage induced by ROS-modulating agents with the ability to target DNA: a comparison of the biological characteristics of citrus pectin and apple pectin. Sci Rep 8:13902. https://doi.org/10.1038/s41598-018-32308-2.
49. Becker K, Tilley L, Vennerstrom JL, Roberts D, Rogerson S, Ginsburg H. 2004. Oxidative stress in malaria parasite-infected erythrocytes: host-parasite interactions. Int J Parasitol 34:163–189. https://doi.org/10.1016/j.ijpara.2003.09.011.
50. Cui L, Miao J, Cui L. 2007. Cytotoxic effect of curcumin on malaria parasite Plasmodium falciparum: inhibition of histone acetylation and generation of reactive oxygen species. Antimicrob Agents Chemother 51:488–494. https://doi.org/10.1128/AAC.01238-06.
51. Pabon NA, Xia Y, Estabrooks SK, Ye Z, Herbrand AK, Süß E, Biondi RM, Assimon VA, Gestwicki JE, Brodsky JL, Camacho CJ, Bar-Joseph Z. 2018.

Predicting protein targets for drug-like compounds using transcriptomics. PLoS Comput Biol 14:e1006651. https://doi.org/10.1371/journal.pcbi.1006651.
52. Mata-Cantero L, Lafuente MJ, Sanz L, Rodriguez MS. 2014. Magnetic isolation of Plasmodium falciparum schizonts iRBCs to generate a high parasitaemia and synchronized in vitro culture. Malar J 13:112. https://doi.org/10.1186/1475-2875-13-112.
53. Subramanian G, Sadeer A, Mukherjee K, Kojima T, Tripathi P, Naidu R, Tay SW, Pang JH, Pullarkat SA, Chandramohanadas R. 2019. Evaluation of ferrocenyl phosphines as potent antimalarials targeting the digestive vacuole function of Plasmodium falciparum. Dalton Trans 48:1108–1117. https://doi.org/10.1039/c8dt04263b.
54. Subramanian G, Babu Rajeev CP, Mohan CD, Sinha A, Chu TTT, Anusha S, Ximei H, Fuchs JE, Bender A, Rangappa KS, Chandramohanadas R, Basappa. 2016. Synthesis and in vitro evaluation of hydrazinyl phthalazines against malaria parasite, Plasmodium falciparum. Bioorg Med Chem Lett 26:3300–3306. https://doi.org/10.1016/j.bmcl.2016.05.049.
55. Chandramohanadas R, Davis PH, Beiting DP, Harbut MB, Darling C, Velmourougane G, Lee MY, Greer PA, Roos DS, Greenbaum DC. 2009. Apicomplexan parasites co-opt host calpains to facilitate their escape from infected cells. Science 324:794–797. https://doi.org/10.1126/science.1171085.
56. Wood DK, Weingeist DM, Bhatia SN, Engelward BP. 2010. Single cell trapping and DNA damage analysis using microwell arrays. Proc Natl Acad Sci U S A 107:10008–10013. https://doi.org/10.1073/pnas.1004056107.
57. Ge J, Wood DK, Weingeist DM, Bhatia SN, Engelward BP. 2012. CometChip: single-cell microarray for high-throughput detection of DNA damage. Methods Cell Biol 112:247–268. https://doi.org/10.1016/B978-0-12-405914-6.00013-5.
58. Mondragon R, Frixione E. 1996. Ca(2+)-dependence of conoid extrusion in Toxoplasma gondii tachyzoites. J Eukaryot Microbiol 43:120–127. https://doi.org/10.1111/j.1550-7408.1996.tb04491.x.
59. Eidell KP, Burke T, Gubbels MJ. 2010. Development of a screen to dissect Toxoplasma gondii egress. Mol Biochem Parasitol 171:97–103. https://doi.org/10.1016/j.molbiopara.2010.03.004.
60. Boyle MJ, Wilson DW, Richards JS, Riglar DT, Tetteh KK, Conway DJ, Ralph SA, Baum J, Beeson JG. 2010. Isolation of viable Plasmodium falciparum merozoites to define erythrocyte invasion events and advance vaccine and drug development. Proc Natl Acad Sci U S A 107:14378–14383. https://doi.org/10.1073/pnas.1009198107.